

High-statistics study of neutral-pion pair production in two-photon collisions

I. Adachi,¹⁰ H. Aihara,⁵¹ K. Arinstein,¹ T. Aso,⁵⁵ V. Aulchenko,¹ T. Aushev,^{22,16}
 T. Aziz,⁴⁷ S. Bahinipati,³ A. M. Bakich,⁴⁶ V. Balagura,¹⁶ Y. Ban,³⁸ E. Barberio,²⁵
 A. Bay,²² I. Bedny,¹ K. Belous,¹⁵ V. Bhardwaj,³⁷ U. Bitenc,¹⁷ S. Blyth,²⁹ A. Bondar,¹
 A. Bozek,³¹ M. Bračko,^{24,17} J. Brodzicka,^{10,31} T. E. Browder,⁹ M.-C. Chang,⁴ P. Chang,³⁰
 Y.-W. Chang,³⁰ Y. Chao,³⁰ A. Chen,²⁸ K.-F. Chen,³⁰ B. G. Cheon,⁸ C.-C. Chiang,³⁰
 R. Chistov,¹⁶ I.-S. Cho,⁵⁷ S.-K. Choi,⁷ Y. Choi,⁴⁵ Y. K. Choi,⁴⁵ S. Cole,⁴⁶ J. Dalseno,¹⁰
 M. Danilov,¹⁶ A. Das,⁴⁷ M. Dash,⁵⁶ A. Drutskoy,³ W. Dungen,¹⁴ S. Eidelman,¹
 D. Epifanov,¹ S. Esen,³ S. Fratina,¹⁷ H. Fujii,¹⁰ M. Fujikawa,²⁷ N. Gabyshev,¹
 A. Garmash,³⁹ P. Goldenzweig,³ B. Golob,^{23,17} M. Grosse Perdekamp,^{12,40} H. Guler,⁹
 H. Guo,⁴² H. Ha,¹⁹ J. Haba,¹⁰ K. Hara,²⁶ T. Hara,³⁶ Y. Hasegawa,⁴⁴ N. C. Hastings,⁵¹
 K. Hayasaka,²⁶ H. Hayashii,²⁷ M. Hazumi,¹⁰ D. Heffernan,³⁶ T. Higuchi,¹⁰ H. Hödlmoser,⁹
 T. Hokuue,²⁶ Y. Horii,⁵⁰ Y. Hoshi,⁴⁹ K. Hoshina,⁵⁴ W.-S. Hou,³⁰ Y. B. Hsiung,³⁰
 H. J. Hyun,²¹ Y. Igarashi,¹⁰ T. Iijima,²⁶ K. Ikado,²⁶ K. Inami,²⁶ A. Ishikawa,⁴¹ H. Ishino,⁵²
 R. Itoh,¹⁰ M. Iwabuchi,⁶ M. Iwasaki,⁵¹ Y. Iwasaki,¹⁰ C. Jacoby,²² N. J. Joshi,⁴⁷ M. Kaga,²⁶
 D. H. Kah,²¹ H. Kaji,²⁶ H. Kakuno,⁵¹ J. H. Kang,⁵⁷ P. Kapusta,³¹ S. U. Kataoka,²⁷
 N. Katayama,¹⁰ H. Kawai,² T. Kawasaki,³³ A. Kibayashi,¹⁰ H. Kichimi,¹⁰ H. J. Kim,²¹
 H. O. Kim,²¹ J. H. Kim,⁴⁵ S. K. Kim,⁴³ Y. I. Kim,²¹ Y. J. Kim,⁶ K. Kinoshita,³
 S. Korpar,^{24,17} Y. Kozakai,²⁶ P. Križan,^{23,17} P. Krokovny,¹⁰ R. Kumar,³⁷ E. Kurihara,²
 Y. Kuroki,³⁶ A. Kuzmin,¹ Y.-J. Kwon,⁵⁷ S.-H. Kyeong,⁵⁷ J. S. Lange,⁵ G. Leder,¹⁴
 J. Lee,⁴³ J. S. Lee,⁴⁵ M. J. Lee,⁴³ S. E. Lee,⁴³ T. Lesiak,³¹ J. Li,⁹ A. Limosani,²⁵
 S.-W. Lin,³⁰ C. Liu,⁴² Y. Liu,⁶ D. Liventsev,¹⁶ J. MacNaughton,¹⁰ F. Mandl,¹⁴
 D. Marlow,³⁹ T. Matsumura,²⁶ A. Matyja,³¹ S. McOnie,⁴⁶ T. Medvedeva,¹⁶ Y. Mikami,⁵⁰
 K. Miyabayashi,²⁷ H. Miyata,³³ Y. Miyazaki,²⁶ R. Mizuk,¹⁶ G. R. Moloney,²⁵ T. Mori,²⁶
 T. Nagamine,⁵⁰ Y. Nagasaka,¹¹ Y. Nakahama,⁵¹ I. Nakamura,¹⁰ E. Nakano,³⁵ M. Nakao,¹⁰
 H. Nakayama,⁵¹ H. Nakazawa,²⁸ Z. Natkaniec,³¹ K. Neichi,⁴⁹ S. Nishida,¹⁰ K. Nishimura,⁹
 Y. Nishio,²⁶ I. Nishizawa,⁵³ O. Nitoh,⁵⁴ S. Noguchi,²⁷ T. Nozaki,¹⁰ A. Ogawa,⁴⁰
 S. Ogawa,⁴⁸ T. Ohshima,²⁶ S. Okuno,¹⁸ S. L. Olsen,^{9,13} S. Ono,⁵² W. Ostrowicz,³¹
 H. Ozaki,¹⁰ P. Pakhlov,¹⁶ G. Pakhlova,¹⁶ H. Palka,³¹ C. W. Park,⁴⁵ H. Park,²¹
 H. K. Park,²¹ K. S. Park,⁴⁵ N. Parslow,⁴⁶ L. S. Peak,⁴⁶ M. Pernicka,¹⁴ R. Pestotnik,¹⁷
 M. Peters,⁹ L. E. Piilonen,⁵⁶ A. Poluektov,¹ J. Rorie,⁹ M. Rozanska,³¹ H. Sahoo,⁹
 Y. Sakai,¹⁰ N. Sasao,²⁰ K. Sayeed,³ T. Schietinger,²² O. Schneider,²² P. Schönmeier,⁵⁰
 J. Schümann,¹⁰ C. Schwanda,¹⁴ A. J. Schwartz,³ R. Seidl,^{12,40} A. Sekiya,²⁷ K. Senyo,²⁶
 M. E. Sevir,²⁵ L. Shang,¹³ M. Shapkin,¹⁵ V. Shebalin,¹ C. P. Shen,⁹ H. Shibuya,⁴⁸
 S. Shinomiya,³⁶ J.-G. Shiu,³⁰ B. Shwartz,¹ J. B. Singh,³⁷ A. Sokolov,¹⁵ A. Somov,³
 S. Stanič,³⁴ M. Starič,¹⁷ J. Stypula,³¹ A. Sugiyama,⁴¹ K. Sumisawa,¹⁰ T. Sumiyoshi,⁵³
 S. Suzuki,⁴¹ S. Y. Suzuki,¹⁰ O. Tajima,¹⁰ F. Takasaki,¹⁰ K. Tamai,¹⁰ N. Tamura,³³
 M. Tanaka,¹⁰ N. Taniguchi,²⁰ G. N. Taylor,²⁵ Y. Teramoto,³⁵ I. Tikhomirov,¹⁶
 K. Trabelsi,¹⁰ Y. F. Tse,²⁵ T. Tsuboyama,¹⁰ Y. Uchida,⁶ S. Uehara,¹⁰ Y. Ueki,⁵³ K. Ueno,³⁰
 T. Uglov,¹⁶ Y. Unno,⁸ S. Uno,¹⁰ P. Urquijo,²⁵ Y. Ushiroda,¹⁰ Y. Usov,¹ G. Varner,⁹

K. E. Varvell,⁴⁶ K. Vervink,²² S. Villa,²² A. Vinokurova,¹ C. C. Wang,³⁰ C. H. Wang,²⁹
J. Wang,³⁸ M.-Z. Wang,³⁰ P. Wang,¹³ X. L. Wang,¹³ M. Watanabe,³³ Y. Watanabe,¹⁸
R. Wedd,²⁵ J.-T. Wei,³⁰ J. Wicht,¹⁰ L. Widhalm,¹⁴ J. Wiechczynski,³¹ E. Won,¹⁹
B. D. Yabsley,⁴⁶ A. Yamaguchi,⁵⁰ H. Yamamoto,⁵⁰ M. Yamaoka,²⁶ Y. Yamashita,³²
M. Yamauchi,¹⁰ C. Z. Yuan,¹³ Y. Yusa,⁵⁶ C. C. Zhang,¹³ L. M. Zhang,⁴² Z. P. Zhang,⁴²
V. Zhilich,¹ V. Zhulanov,¹ T. Zivko,¹⁷ A. Zupanc,¹⁷ N. Zwahlen,²² and O. Zyukova¹

(The Belle Collaboration)

¹*Budker Institute of Nuclear Physics, Novosibirsk*

²*Chiba University, Chiba*

³*University of Cincinnati, Cincinnati, Ohio 45221*

⁴*Department of Physics, Fu Jen Catholic University, Taipei*

⁵*Justus-Liebig-Universität Gießen, Gießen*

⁶*The Graduate University for Advanced Studies, Hayama*

⁷*Gyeongang National University, Chinju*

⁸*Hanyang University, Seoul*

⁹*University of Hawaii, Honolulu, Hawaii 96822*

¹⁰*High Energy Accelerator Research Organization (KEK), Tsukuba*

¹¹*Hiroshima Institute of Technology, Hiroshima*

¹²*University of Illinois at Urbana-Champaign, Urbana, Illinois 61801*

¹³*Institute of High Energy Physics,*

Chinese Academy of Sciences, Beijing

¹⁴*Institute of High Energy Physics, Vienna*

¹⁵*Institute of High Energy Physics, Protvino*

¹⁶*Institute for Theoretical and Experimental Physics, Moscow*

¹⁷*J. Stefan Institute, Ljubljana*

¹⁸*Kanagawa University, Yokohama*

¹⁹*Korea University, Seoul*

²⁰*Kyoto University, Kyoto*

²¹*Kyungpook National University, Taegu*

²²*École Polytechnique Fédérale de Lausanne (EPFL), Lausanne*

²³*Faculty of Mathematics and Physics, University of Ljubljana, Ljubljana*

²⁴*University of Maribor, Maribor*

²⁵*University of Melbourne, School of Physics, Victoria 3010*

²⁶*Nagoya University, Nagoya*

²⁷*Nara Women's University, Nara*

²⁸*National Central University, Chung-li*

²⁹*National United University, Miao Li*

³⁰*Department of Physics, National Taiwan University, Taipei*

³¹*H. Niewodniczanski Institute of Nuclear Physics, Krakow*

³²*Nippon Dental University, Niigata*

³³*Niigata University, Niigata*

³⁴*University of Nova Gorica, Nova Gorica*

³⁵*Osaka City University, Osaka*

³⁶*Osaka University, Osaka*

³⁷*Panjab University, Chandigarh*

³⁸*Peking University, Beijing*

- ³⁹*Princeton University, Princeton, New Jersey 08544*
⁴⁰*RIKEN BNL Research Center, Upton, New York 11973*
⁴¹*Saga University, Saga*
⁴²*University of Science and Technology of China, Hefei*
⁴³*Seoul National University, Seoul*
⁴⁴*Shinshu University, Nagano*
⁴⁵*Sungkyunkwan University, Suwon*
⁴⁶*University of Sydney, Sydney, New South Wales*
⁴⁷*Tata Institute of Fundamental Research, Mumbai*
⁴⁸*Toho University, Funabashi*
⁴⁹*Tohoku Gakuin University, Tagajo*
⁵⁰*Tohoku University, Sendai*
⁵¹*Department of Physics, University of Tokyo, Tokyo*
⁵²*Tokyo Institute of Technology, Tokyo*
⁵³*Tokyo Metropolitan University, Tokyo*
⁵⁴*Tokyo University of Agriculture and Technology, Tokyo*
⁵⁵*Toyama National College of Maritime Technology, Toyama*
⁵⁶*Virginia Polytechnic Institute and State University, Blacksburg, Virginia 24061*
⁵⁷*Yonsei University, Seoul*

Abstract

The differential cross section for the process $\gamma\gamma \rightarrow \pi^0\pi^0$ has been measured in the kinematic range $0.6 \text{ GeV} < W < 4.1 \text{ GeV}$, $|\cos\theta^*| < 0.8$ in energy and pion scattering angle, respectively, in the $\gamma\gamma$ center-of-mass system. The results are based on a 223 fb^{-1} data sample collected with the Belle detector at the KEKB e^+e^- collider. Using the data with $W > 1.4 \text{ GeV}$, we obtain results on light-quark resonances and charmonia. We also compare the observed angular dependence and ratios of cross sections for neutral-pair and charged-pair production to QCD models. Differential cross sections are fitted in the energy region, $1.4 \text{ GeV} < W < 2.2 \text{ GeV}$, with a simple model where partial waves consist of resonances such as $f_2'(1525)$, $f_2(1950)$ and $f_4(2050)$ and smooth backgrounds. In the higher energy region, we observe production of the χ_{c0} charmonium state and obtain the product of its two-photon decay width and the branching fraction to $\pi^0\pi^0$. The energy and angular dependences above 3.1 GeV are compatible with those measured in the $\pi^+\pi^-$ channel, and in addition we find that the cross section ratio, $\sigma(\pi^0\pi^0)/\sigma(\pi^+\pi^-)$, is $0.32 \pm 0.03 \pm 0.05$ on average in the $3.1\text{-}4.1 \text{ GeV}$ region.

PACS numbers: 13.20.Gd, 13.60.Le, 13.66.Bc, 14.40.Cs, 14.40.Gx

I. INTRODUCTION

Measurements of exclusive hadronic final states in two-photon collisions provide valuable information concerning physics of light and heavy-quark resonances, perturbative and non-perturbative QCD and hadron-production mechanisms. So far, we have measured the production cross sections for charged-pion pairs [1, 2], charged- and neutral-kaon pairs [2, 3], and proton-antiproton pairs [4]. We have also analyzed D -meson-pair production and observe a new charmonium state [5]. Recently, we have presented a measurement of neutral-pion pair production based on a data sample corresponding to an integrated luminosity of 95 fb^{-1} [6]. We have carried out an analysis to extract information on light quark resonances from the energy and angular dependences of the differential cross sections (DCS), by fitting to the resonance parameters of $f_0(980)$, $f_2(1270)$ and other hypothetical resonances.

Here we present a measurement of the DCS, $d\sigma/d|\cos\theta^*|$, for the process $\gamma\gamma \rightarrow \pi^0\pi^0$ in a wide two-photon center-of-mass (c.m.) energy (W) range from 0.6 to 4.1 GeV, and in the c.m. angular range, $|\cos\theta^*| < 0.8$. We use a 223 fb^{-1} data sample, which is more than twice as large as that in our previous analysis [6, 7]. We focus on the range $W > 1.4 \text{ GeV}$, where the previous data was statistically limited.

In the intermediate energy range ($1.0 \text{ GeV} < W < 2.4 \text{ GeV}$), the formation of meson resonances decaying to $\pi\pi$ is the dominant contribution. For ordinary $q\bar{q}$ mesons in isospin conserving decays to $\pi\pi$, the only allowed $I^G J^{PC}$ states produced by two photons are $0^+(\text{even})^{++}$, that is, $f_{J=\text{even}}$ mesons. Several mesons with these quantum numbers are suggested by results of hadron-beam or charmonium decay experiments in the 1.5 - 2.2 GeV region, but none of them have been firmly established in two-photon processes, which are sensitive to the internal quark structure of the meson. In addition, the $\pi^0\pi^0$ channel has two advantages in the study of resonances: a smaller contribution from the continuum is expected in it than in the $\pi^+\pi^-$ channel; and the angular coverage is larger ($|\cos\theta^*| < 0.8$ instead of 0.6).

At higher energies, we can invoke a quark model. In leading order calculations [8, 9], which take into account the spin correlation between quarks, the $\pi^0\pi^0$ cross section is predicted to be much smaller than that of $\pi^+\pi^-$, and the ratio of $\pi^0\pi^0$ to $\pi^+\pi^-$ cross sections is around 0.03-0.06. However, higher-order or non-perturbative QCD effects can modify this ratio. For example, the handbag model, which considers soft hadron exchange, predicts the same amplitude for the two processes, and thus the expected ratio is 0.5 [10]. Analyses of energy and angular distributions of the cross sections are essential for determining properties of the observed resonances and for testing the validity of QCD models.

The organization of this article is as follows. In Section II, a brief description of the Belle detector is given. Section III explains the procedure used to obtain differential cross sections. Section IV is devoted to results on resonances obtained by fitting differential cross sections in the range $1.4 \text{ GeV} < W < 2.2 \text{ GeV}$. Section V describes analyses at higher energy. The topics included there are the angular dependence as a function of W , the charmonia χ_{c0} and χ_{c2} states and the ratio of $\pi^0\pi^0$ to $\pi^+\pi^-$ cross sections. Finally, Section VI concludes this report. All of the results presented in this report are preliminary.

II. EXPERIMENTAL APPARATUS

We use a 223 fb^{-1} data sample from the Belle experiment [11] at the KEKB accelerator [12]. The data were recorded at e^+e^- c.m. energies of 10.58 GeV (179 fb^{-1}), 10.52 GeV

(19 fb⁻¹), 10.36 GeV ($\Upsilon(3S)$ runs, 2.9 fb⁻¹), 10.30 GeV (0.3 fb⁻¹) and 10.86 GeV ($\Upsilon(5S)$ runs, 21.7 fb⁻¹). The difference of two-photon fluxes per e^+e^- -beam luminosity (=luminosity function) in the measured W regions due to the difference of the beam energies is small (maximum $\pm 4\%$). We combine the results from the different beam energies. The effect on the cross section is less than 0.5%.

The analysis is carried out in the “zero-tag” mode, where neither the recoil electron nor positron are detected. We restrict the virtuality of the incident photons to be small by imposing strict transverse-momentum balance with respect to the beam axis for the final-state hadronic system.

A comprehensive description of the Belle detector is given elsewhere [11]. We mention here only those detector components that are essential for the present measurement. Charged tracks are reconstructed from hit information in a silicon vertex detector and a central drift chamber (CDC) located in a uniform 1.5 T solenoidal magnetic field. The detector solenoid is oriented along the z axis, which points in the direction opposite to that of the positron beam. Photon detection and energy measurements are performed with a CsI(Tl) electromagnetic calorimeter (ECL).

For this all-neutral final state, we require that there be no reconstructed tracks coming from the vicinity of the nominal collision point. Therefore, the CDC is used for vetoing events with charged track(s). Photons from decays of two neutral pions are detected and their momentum vectors are measured by the ECL. Signals from the ECL are also used to trigger signal events.

III. DERIVING DIFFERENTIAL CROSS SECTIONS

The event triggers, data processing, and event selection are the same as those described in Ref. [6]. We derive the c.m. energy W of the two-photon collision from the invariant mass of the two neutral pion system. We calculate the cosine of the scattering angle of π^0 in the $\gamma\gamma$ c.m. frame, $|\cos\theta^*|$ for each event, using the e^+e^- collision axis in the e^+e^- c.m. frame as the reference of the polar angle as an approximation, because we do not know the exact $\gamma\gamma$ collision axis.

A. Data reduction

We find that the signal candidates in the low energy region ($W < 1.2$ GeV) are considerably contaminated by background events. We study the p_t -balance distribution, i.e., the event distribution in $|\sum \mathbf{p}_t^*|$, to separate the signal and background components. We estimate the p_t -unbalanced background component for $W < 1.2$ GeV, and subtract the yield in the signal region, in the same manner as in the previous analysis [6]. However, above 1.2 GeV, we cannot quantitatively determine the background contamination because of the small background rate and low statistics of the sample, as well as the uncertainty in the functional form for the signal shape.

Using the ratio of yields between the p_t -balanced and unbalanced regions, we can estimate the backgrounds. In Fig. 1, we plot the W dependences of

$$R = \text{Yield}(0.15 < |\sum \mathbf{p}_t^*| < 0.20 \text{ GeV}/c) / \text{Yield}(|\sum \mathbf{p}_t^*| < 0.05 \text{ GeV}/c). \quad (1)$$

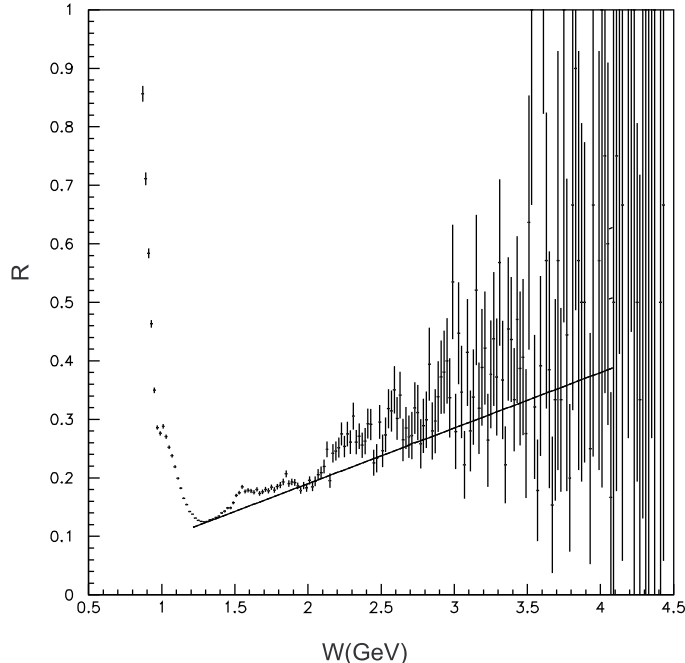


FIG. 1: The yield ratio R in the p_t -unbalanced bin to the p_t -balanced (signal) bin (see text for the exact definition) for the experimental data. The solid line shows the signal-component obtained from the signal-MC and corrected taking into account the poorer momentum resolution in experimental data.

We integrate over all angles in this figure. The main part of the W -dependence of R comes from the energy dependence of the momentum resolution. The expected ratio from the pure signal component (calculated from the signal Monte Carlo (MC) events and corrected for the deviation of the p_t resolution discussed in the next subsection) is shown by the solid line. The excess of R over the line (ΔR) is expected to correspond to the contribution from the p_t -unbalanced background. The excess is relatively small above 1.0 GeV, although some fine structure is visible there. In the range 1.2-1.5 GeV, ΔR is undetectably small; for 1.5-3.3 GeV, ΔR ranges between 0.00 and 0.08; above 3.3 GeV, ΔR is the range from 0.08 to 0.2. From the R values, we estimate that the background contamination in the signal region is $\sim R/4$, which is smaller than 3% for 1.1 - 3.3 GeV and around 3% for 3.6 - 4.1 GeV. We subtract 3% for 3.6 - 4.1 GeV, and assign a 3% systematic error from this source for the 1.5 - 4.1 GeV range.

We estimate the invariant-mass resolution from studies of signal-MC and experimental events. We find that an asymmetric Gaussian function with standard deviations of $1.9\%W$ and $1.3\%W$ on the lower and higher sides of the peak, respectively, approximates the smearing reasonably well. Based on this information, unfolding is performed using the singular value decomposition (SVD) algorithm [13] at the yield level [6], and is applied to obtain the corrected W distribution in the 0.9 - 2.4 GeV region, using data with observed W values between 0.72 and 2.68 GeV. For lower energies, $W < 0.9$ GeV, the effect of the migration is expected to be small because the invariant-mass resolution is small compared with the bin width. For higher energies, $W > 2.4$ GeV, where the statistics is relatively low and unfolding would enlarge the errors, we rebin events into 100 MeV bins without unfolding.

B. Calculation of differential cross section

We determine the trigger efficiency for signal using the detector and trigger simulators applied to the signal MC events. The signal MC data for $e^+e^- \rightarrow e^+e^-\pi^0\pi^0$ are generated using the TREPS code [14] for the efficiency determination, isotropically in $|\cos\theta^*|$ at 58 fixed W points between 0.5 and 4.5 GeV. The angular distribution at the generator level does not play a role in the efficiency determination, because we calculate the efficiencies separately in each $|\cos\theta^*|$ bin with a 0.05 width. Samples of 4×10^5 events are generated at each W point. Two sets of different background conditions, which were extracted from the beam collision data are embedded in the signal MC data in the detector simulation; these are put through the trigger simulator and the event selection program. To minimize statistical fluctuations in the MC calculation, we fit the numerical results of the trigger efficiency to a two-dimensional empirical function in $(W, |\cos\theta^*|)$.

The efficiency calculated from the signal MC events is corrected for a systematic difference of the peak widths in the p_t -balance distributions found between the experimental data and the MC events, which is attributed to a difference in the momentum resolution for π^0 's. The correction factor is typically 0.95.

The DCS for each $(W, |\cos\theta^*|)$ point is derived from the following formula:

$$\frac{d\sigma}{d|\cos\theta^*|} = \frac{\Delta Y - \Delta B}{\Delta W \Delta|\cos\theta^*| \int \mathcal{L} dt L_{\gamma\gamma}(W) \eta}, \quad (2)$$

where ΔY and ΔB are the signal yield and the estimated p_t -unbalanced background in the bin, ΔW and $\Delta|\cos\theta^*|$ are the bin widths, $\int \mathcal{L} dt$ and $L_{\gamma\gamma}(W)$ are the integrated luminosity and two-photon luminosity function calculated by TREPS [14], respectively, and η is the efficiency including the correction described above. The energy bin width ΔW is 0.02 GeV for $0.6 \text{ GeV} < W < 1.8 \text{ GeV}$, 0.04 GeV for $1.8 \text{ GeV} < W < 2.4 \text{ GeV}$, and 0.1 GeV for $2.4 \text{ GeV} < W < 4.1 \text{ GeV}$. The width of each angular bin is $\Delta|\cos\theta^*| = 0.05$.

Figure 2 shows the W dependence of the cross section integrated over $|\cos\theta^*| < 0.8$. The results are obtained by simply summing $d\sigma/d|\cos\theta^*| \cdot \Delta|\cos\theta^*|$ over the corresponding angular bins. We have removed the bins in the range $3.3 \text{ GeV} < W < 3.6 \text{ GeV}$, because we cannot separate the χ_{c0} and χ_{c2} components and the continuum in a model-independent way due to the finite mass resolution and insufficient statistics of the measurement. The cross section in this region is discussed in detail in Section V.

We show the angular dependence of the DCS at several W points in Fig. 3. Note that the cross sections in the neighboring bins after the unfolding are no longer independent of each other in both central values and size of errors.

We estimate the systematic errors for the cross section in each energy bin arising from various sources. The systematic errors arise from uncertainties in trigger efficiency (4-30%), π^0 reconstruction efficiency (6%), p_t -balance cut (typically 3%), background subtraction (0-40%), luminosity function (4-5%), beam background effect for efficiency (2-4%), other efficiency errors (4%) and the unfolding procedure (0-4%), for which we show a range when the relative error size depends on W . The total systematic error is obtained by adding the uncertainties in quadrature and is 10% in the intermediate W region. The systematic error becomes much larger at lower W . At higher W , the systematic error is rather stable, typically $\sim 11\%$.

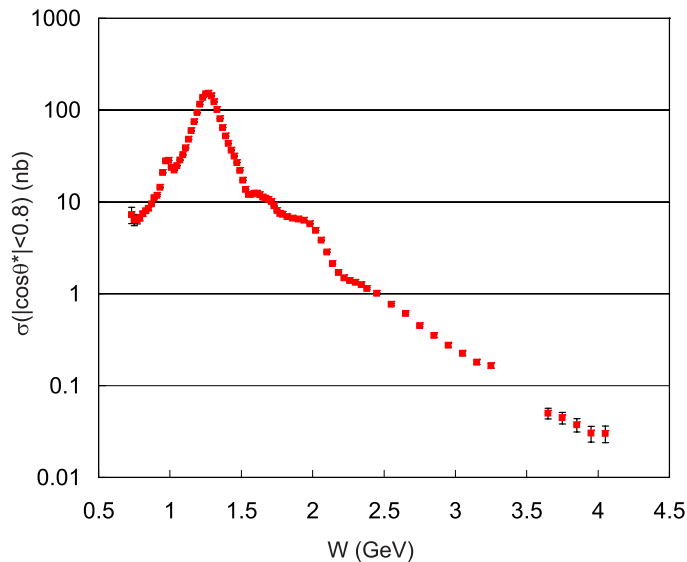


FIG. 2: The integrated cross section results in the angular regions $|\cos\theta^*| < 0.8$. Data points in bins near 3.5 GeV are not shown because of uncertainty from the χ_{cJ} subtraction.

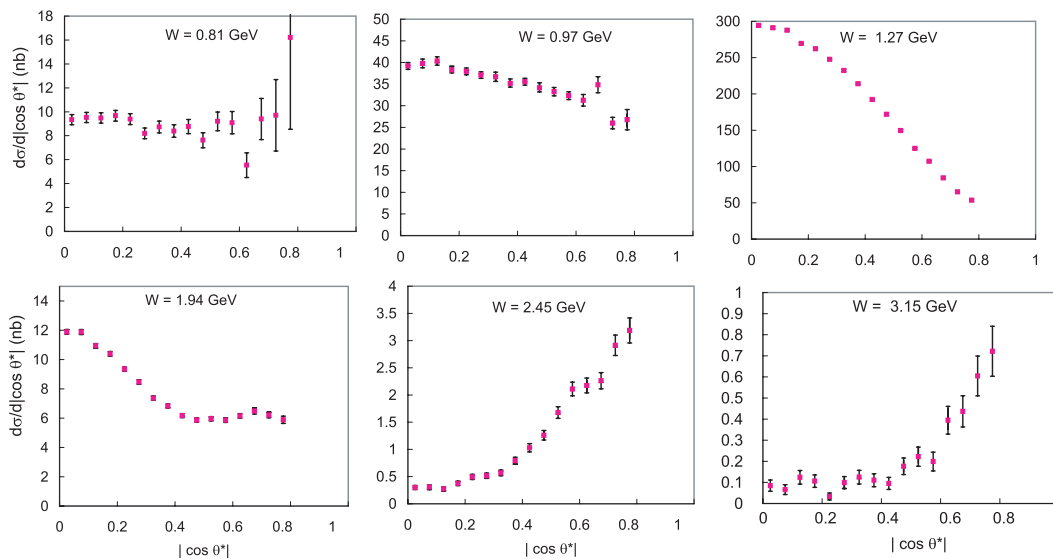


FIG. 3: The DCS for five selected W points, 0.97 GeV, 1.27 GeV, 1.95 GeV, 2.45 GeV and 3.15 GeV.

IV. ANALYSIS OF RESONANCES IN THE RANGE $1.4 \text{ GeV} < W < 2.2 \text{ GeV}$

Previously, we have obtained a reasonable fit to a simple model of resonances and smooth backgrounds in the energy region $0.8 \text{ GeV} < W < 1.6 \text{ GeV}$ from the DCS of $\gamma\gamma \rightarrow \pi^0\pi^0$ with a 95 fb^{-1} data sample [6]. The clear $f_0(980)$ peak and the large contribution from the $f_2(1270)$ can be fitted with parameters determined from $\pi^+\pi^-$ data [1].

In this section, we extend the analysis to the higher energy region $1.4 \text{ GeV} < W < 2.2 \text{ GeV}$ (which has some overlap with the previous study) using a higher statistics sample of 223 fb^{-1} . It is well known that deriving reliable results on partial waves is difficult,

especially in the higher energy region considered here. The goal of this study is to provide some information on partial waves in this energy region and to demonstrate the sensitivity (and limitations) of our high-statistics data sample (three orders of magnitude more statistics than the past experiments) with a large angular coverage ($|\cos\theta^*| \leq 0.8$).

A. Parameterization of Partial Wave Amplitudes

In the energy region $W \leq 3$ GeV, $J > 4$ partial waves (next is $J = 6$) may be neglected so that only S, D and G waves are to be considered. The DCS can be expressed as:

$$\frac{d\sigma}{d\Omega}(\gamma\gamma \rightarrow \pi^0\pi^0) = \left|S Y_0^0 + D_0 Y_2^0 + G_0 Y_4^0\right|^2 + \left|D_2 Y_2^2 + G_2 Y_4^2\right|^2, \quad (3)$$

where D_0 and G_0 (D_2 and G_2) denotes the helicity 0 (2) components of the D and G wave, respectively, and Y_j^m are the spherical harmonics.

We derive some information on resonances in the DCS fit by parameterizing partial wave amplitudes in terms of resonances and smooth “backgrounds”. Once the functional forms of the amplitudes are assumed, we can use Eq. (3) to fit the DCS. From Fig. 10 in Ref. [6] (also from the same plot with higher statistics), it appears that the G waves are non-zero at $W \gtrsim 1.8$ GeV and are dominated by the G_2 wave. Here we assume (and check the necessity of) including the $f_4(2050)$ in the G_2 wave; we note that the $f_4(2050)$ ’s two-photon coupling has not been measured. Since the G_2 wave interferes with the D_2 wave, and the D_2 wave should contain resonances besides the $f_2(1270)$, we include the known resonances, the $f_2'(1525)$ and $f_2(1950)$, which are known to couple to two photons (while the $f_2(2010)$ does not). There are several more resonances that might couple to $\gamma\gamma$ and $\pi\pi$ in this mass region as listed in Ref. [15]. Thus we assume that the $f_2(1950)$ is just an empirical parameterization representing these other resonances; we denote it as the “ $f_2(1950)$ ”.

We parameterize the partial waves as follows:

$$\begin{aligned} S &= A_{f_0(Y)} e^{i\phi_{sY}} + B_S, \\ D_0 &= \sqrt{\frac{r_{02}}{1+r_{02}}} A_{f_2(1270)} e^{i\phi_{d0}} + B_{D0}, \\ D_2 &= \sqrt{\frac{1}{1+r_{02}}} A_{f_2(1270)} e^{i\phi_{d2}} + A_{f_2'(1525)} e^{i\phi_{2p}} + A_{f_2(Z)} e^{i\phi_{2z}} + A_{f_2(1950)''} e^{i\phi_{29}} + B_{D2}, \\ G_0 &= 0, \\ G_2 &= A_{f_4(2050)} e^{i\phi_4} + B_{G2} \end{aligned} \quad (4)$$

where $A_{f_0(Y)}$, $A_{f_2(1270)}$, $A_{f_2'(1525)}$, $A_{f_2(Z)}$, $A_{f_2(1950)''}$ and $A_{f_4(2050)}$ are the amplitudes of the corresponding resonances; B_S , B_{D0} , B_{D2} and B_{G2} are “background” amplitudes for S, D_0 , D_2 and G_2 waves; r_{02} is the helicity-0 fraction of the $f_2(1270)$; and ϕ_{sY} , ϕ_{d0} , ϕ_{d2} , ϕ_{2p} , ϕ_{2z} , ϕ_{29} and ϕ_4 are the phases of resonances relative to background amplitudes. An $f_0(Y)$ term was needed to obtain a good fit in the previous analysis of the energy region 0.8 GeV $< W < 1.6$ GeV [6]. The $f_2(Z)$ is needed here to “explain” the dip-bump structure in the range 1.5 GeV $< W < 1.7$ GeV as seen in Fig. 2. We assume that $G_0 = 0$ and that G_2 consists only of the $f_4(2050)$ and a smooth “background”.

TABLE I: Parameters of the $f'_2(1525)$, $f_2(1950)$ and $f_4(2050)$ [15].

Parameter	$f'_2(1525)$	$f_2(1950)$	$f_4(2050)$	Unit
Mass	1525 ± 5	1944 ± 12	2025 ± 10	MeV/ c^2
Width	73^{+6}_{-5}	472 ± 18	225 ± 18	MeV
$\mathcal{B}(\pi\pi)$	0.82 ± 0.15	seen	17.0 ± 1.5	%
$\mathcal{B}(K\bar{K})$	88.8 ± 3.1	seen	$0.68^{+0.34}_{-0.18}$	%
$\mathcal{B}(\eta\eta)$	10.3 ± 3.1	seen	21 ± 8	%
$\mathcal{B}(\gamma\gamma)$	1.11 ± 0.14	seen	unknown	10^{-6}

We parameterize resonances with the formula given in Eq. (5). The relativistic Breit-Wigner resonance amplitude $A_R(W)$ for a spin- J resonance R of mass m_R is given by

$$A_R^J(W) = \sqrt{\frac{8\pi(2J+1)m_R}{W}} \frac{\sqrt{\Gamma_{\gamma\gamma}\Gamma_{\pi^0\pi^0}}}{m_R^2 - W^2 - im_R\Gamma_{\text{tot}}}. \quad (5)$$

Energy-dependent widths are used for the parameterization of the $f_2(1270)$ and $f'_2(1525)$ [1]. The resonance parameters given in Ref. [15] for the $f'_2(1525)$, $f_2(1950)$ and $f_4(2050)$ are summarized in Table I. Since all (some) of the individual decay fractions of the “ $f_2(1950)$ ” ($f_4(2050)$) are not known, we neglect the W dependence of their partial and total widths.

Background amplitudes are parameterized as follows.

$$\begin{aligned} B_S &= a_{sr}(W - W_0)^2 + b_{sr}(W - W_0) + c_{sr} + i(a_{si}(W - W_0)^2 + b_{si}(W - W_0) + c_{si}), \\ B_{D0} &= a_0(W - W_0)^2 + b_0(W - W_0) + c_0, \\ B_{D2} &= a_2(W - W_0)^2 + b_2(W - W_0) + c_2, \\ B_{G2} &= a_{gr}(W - W_0)^2 + b_{gr}(W - W_0) + c_{gr} + i(a_{gi}(W - W_0)^2 + b_{gi}(W - W_0) + c_{gi}), \end{aligned} \quad (6)$$

where $W_0 = 1.2$ GeV and we fix $c_{gr} = c_{gi} = 0$ to reduce the number of parameters; floating them does not improve fitting. We assume background amplitudes to be quadratic in W for all the waves for both real and imaginary parts. The background D_0 and D_2 amplitudes are taken to be real by definition.

B. Fit results

In the fit, we fix the values of the parameters for the $f_0(Y)$, $f_2(1270)$ and the phases ϕ_{d0} and ϕ_{d2} to those determined in Ref. [1] and [6]. The parameters of the $f'_2(1525)$ are fixed to those in Ref. [15]. If the resonance parameters of the “ $f_2(1950)$ ” and $f_4(2050)$ are fixed at the values given in PDG [15] as summarized in Table I, then the fit is very poor yielding $\chi^2/ndf = 4.0$. Here we quote the results when they are floated. By fixing the phases ϕ_{d0} and ϕ_{d2} , the sign ambiguity for B_{D0} and B_{D2} can be resolved.

Here the unfolded DCS are fitted. One to three thousand sets of randomly generated initial parameters are fitted for each study. Two solutions (denoted by sol. A and B) of

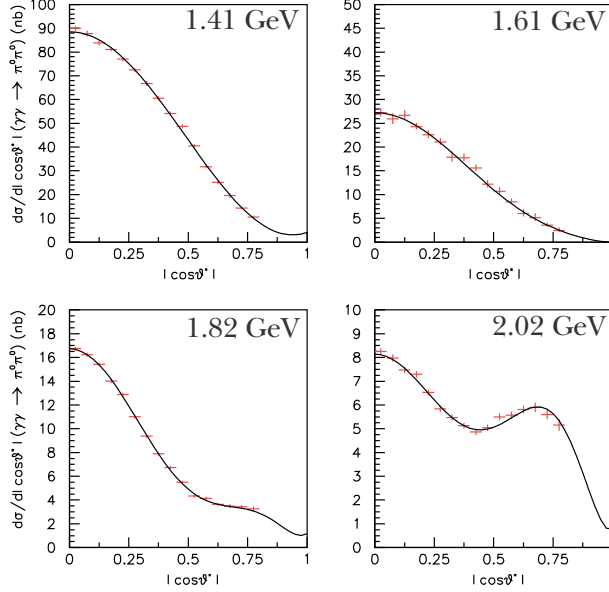


FIG. 4: Fitted curves (solid line) and DCS ($d\sigma/d|\cos\theta^*|$ (nb)) for W -bins indicated.

reasonably good fit quality ($\chi^2/ndf = 1.08$) are obtained only for the nominal fit, where an $f_2(Z)$ component is included together with the “ $f_2(1950)$ ” and $f_4(2050)$, whose parameters are floated. Fit results are shown in Fig. 4 for the DCS and in Fig. 5 for the total cross section. Two solutions are indistinguishable. The main difference between sol. A and B is the two photon coupling of the “ $f_2(1950)$ ” and $f_2(Z)$; that is larger by a factor of 8 (5) in sol. B for the “ $f_2(1950)$ ” ($f_2(Z)$), which may be too large. These two solutions arise from constructive and destructive interference between resonances and backgrounds.

Since the two-photon coupling of the $f_4(2050)$ has not been measured, a fit without it is also given in Table II. The fit quality is unacceptable, indicating that the $f_4(2050)$ has a non-zero two-photon coupling. The existence of the $f_2(Z)$, a spin-2 resonance with mass near $1500 \text{ MeV}/c^2$, is controversial. Thus, fits are also made without the $f_2(Z)$. There, two fits are carried out fixing and floating the branching fraction to two photons of the $f'_2(1525)$. The fitted parameters are listed in Table II. The fit without the $f_2(Z)$ gives an unacceptable χ^2 . When the branching fraction of the $f'_2(1525)$ to two photons is floated with no $f_2(Z)$ contribution, the value obtained is ten times larger than the nominal value, which is unacceptable; thus some resonance like the $f_2(Z)$ is indeed necessary.

The spin of the “resonance” of mass $\sim 1500 \text{ MeV}/c^2$ (denoted here as $f_2(Z)$ for a spin-2 resonance) is not known. Thus we also fit by assuming the spin to be 0 denoted as the $f_0(Z)$, which contributes to the S-wave. In additions, fits with the $f_4(2050)$ only, the “ $f_2(1950)$ ” only and no new resonances are performed; the results are summarized in Table III. The $f_2(Z)$ hypothesis is favored over that of the $f_0(Z)$ with about 3σ significance, which is calculated from the difference of χ^2 values.

A study of systematic errors is not performed because we do not know how to estimate uncertainty from model dependence.

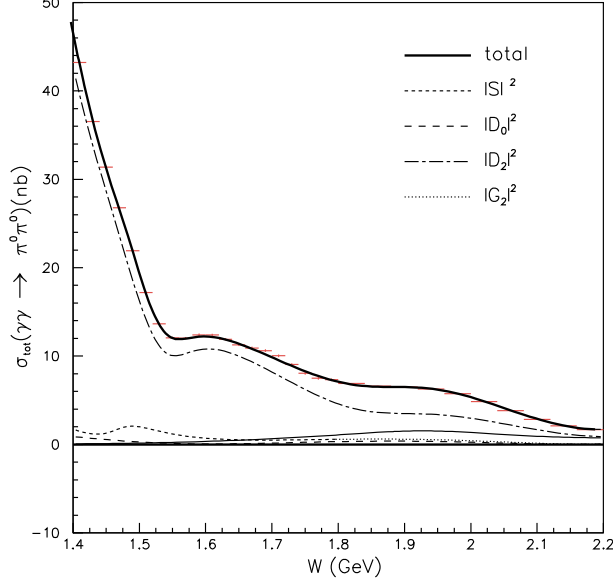


FIG. 5: Total cross section ($|\cos\theta^*| < 0.8$ (nb)) and fitted curves.

TABLE II: Fitted parameters (1)

Parameter	With $f_2(Z)$		Without $f_2(Z)$		Unit	
	All included		no	$\mathcal{B}(f'_2(1525) \rightarrow \gamma\gamma)$		
	sol. A	sol. B	$f_4(2050)$	fixed free		
$\text{Mass}(f_4(2050))$	1935^{+12}_{-14}	1902^{+12}_{-13}	–	1865^{+14}_{-15}	1866 ± 19	MeV/c^2
$\Gamma_{\text{tot}}(f_4(2050))$	369^{+17}_{-22}	350^{+25}_{-22}	–	379^{+34}_{-29}	356^{+32}_{-29}	MeV
$\Gamma_{\gamma\gamma}(f_4(2050))$	45^{+11}_{-19}	74^{+16}_{-13}	0 (fixed)	91^{+32}_{-25}	68 ± 12	eV
$\text{mass}(\text{"}f_2(1950)\text{"})$	1852^{+23}_{-20}	1906^{+8}_{-9}	2191 ± 6	1638^{+8}_{-7}	1741^{+9}_{-12}	MeV/c^2
$\Gamma_{\text{tot}}(\text{"}f_2(1950)\text{"})$	347^{+23}_{-20}	394^{+24}_{-22}	38^{+18}_{-14}	357^{+16}_{-17}	370^{+11}_{-12}	MeV
$\Gamma_{\gamma\gamma}\mathcal{B}(\pi^0\pi^0)$	$9.2^{+4.8}_{-2.6}$	75^{+24}_{-22}	$0.4^{+0.3}_{-0.2}$	$165.9^{+22.2}_{-24.1}$	$50.3^{+54.4}_{-17.0}$	eV
$\text{mass}(f_2(Z))$	1526^{+9}_{-6}	1542^{+7}_{-5}	1649 ± 5	–	–	MeV/c^2
$\Gamma_{\text{tot}}(f_2(Z))$	121 ± 9	217^{+15}_{-16}	414 ± 15	–	–	MeV
$\Gamma_{\gamma\gamma}\mathcal{B}(\pi^0\pi^0)$	$17.5^{+2.8}_{-5.6}$	87 ± 27	503^{+47}_{-40}	0 (fixed)	0 (fixed)	eV
$\mathcal{B}_{f'_2(1525)}(\gamma\gamma)$	1.11 (fixed)				11.9 ± 1.3	10^{-6}
χ^2 (ndf)	485.0 (450)	485.2 (450)	619.1 (454)	571.0 (454)	517.5 (453)	

V. ANALYSIS OF THE HIGHER-ENERGY REGION

In general, we expect that theoretical models based on QCD give reasonable predictions even for two-photon production of exclusive final-states such as $\gamma\gamma \rightarrow \pi^0\pi^0$ in the high energy region. However, the models do not give information on what energies can be considered as high enough.

The handbag model [10] predicts that the angular dependence of the DCS for $\gamma\gamma \rightarrow \pi\pi$ goes as $\sim \sin^{-4}\theta^*$. This prediction is common to charged and neutral pairs of pions. Our measurement for the charged-pion process agrees with this expectation above $W >$

TABLE III: Fitted parameters (2)

Parameter	With $f_0(Z)$	$f_4(2050)$ only	“ $f_2(1950)$ ” only	None	Unit
Mass($f_4(2050)$)	1876^{+11}_{-10}	1894 ± 7	–	–	MeV/ c^2
$\Gamma_{\text{tot}}(f_4(2050))$	493^{+17}_{-20}	268^{+15}_{-13}	–	–	MeV
$\Gamma_{\gamma\gamma}(f_4(2050))$	213^{+42}_{-43}	31^{+8}_{-5}	–	0 (fixed)	eV
Mass(“ $f_2(1950)$ ”)	1752^{+14}_{-9}	–	1630 ± 31	–	MeV/ c^2
$\Gamma_{\text{tot}}(“f_2(1950)”) $	310^{+26}_{-24}	–	362^{+11}_{-9}	–	MeV
$\Gamma_{\gamma\gamma}\mathcal{B}(“f_2(1950)” \rightarrow \pi^0\pi^0)$	$10.0^{+4.9}_{-3.2}$	0 (fixed)	132^{+12}_{-11}	0 (fixed)	eV
Mass($f_0(Z)$)	1566^{+10}_{-13}	–	–	–	MeV/ c^2
$\Gamma_{\text{tot}}(f_0(Z))$	118^{+23}_{-27}	–	–	–	MeV
$\Gamma_{\gamma\gamma}\mathcal{B}(f_0(Z) \rightarrow \pi^0\pi^0)$	91^{+52}_{-39}	0 (fixed)	0 (fixed)	0 (fixed)	eV
$\chi^2(ndf)$	496.3 (450)	1938.6 (458)	705.0 (458)	2950.0 (462)	

3.1 GeV [2]. The prediction of the cross section ratio, $\sigma(\pi^0\pi^0)/\sigma(\pi^+\pi^-)$ is determined by isospin invariance to be 0.5.

However, predictions based on perturbative QCD at leading order suggests that an angular distribution for $\pi^0\pi^0$ will be different from that for $\pi^+\pi^-$. The primary term of the leading order (a short-range emission term) for the charged-pion process is well described by a $\sin^{-4}\theta^*$ dependence [8], while this term vanishes for the neutral-pion process. The shape of the angular distribution from the next term (a long-range interaction term) is unpredictable, and in general, perturbative QCD models predict smaller cross sections for this next term and hence a small neutral to charged cross-section ratio, $\sigma(\pi^0\pi^0)/\sigma(\pi^+\pi^-) \sim 0.03$.

A. Angular dependence

We compare the angular dependence of the DCS in the range $|\cos\theta^*| < 0.8$ for $W > 2.4$ GeV with the function $\sin^{-4}\theta^*$. We also try a fit with an additional term, to quantify a possible deviation from $\sin^{-4}\theta^*$ behavior. We choose this function because it gives relatively good fits empirically in a wide range of W . Thus the fit function is parameterized as:

$$d\sigma/d|\cos\theta^*| = a(\sin^{-4}\theta^* + b\cos^2\theta^*). \quad (7)$$

We fit using a binned maximum likelihood method and 16 bins in the range $|\cos\theta^*| < 0.8$. We know that the effect of charmonia is large in the region $3.2 \text{ GeV} < W < 3.6 \text{ GeV}$, but we cannot separate it in the angular dependence because we cannot assume here any functional shapes for the non-charmonium component. The results of the fit for b are shown in Fig. 6 as well as the fit to the angular distributions in the four selected W regions, where the DCS, the vertical axis of this figure, is normalized to the total cross section $\sigma(|\cos\theta^*| < 0.8)$ in each W region, i.e. the area under the curve is 1. The parameter b is close to zero above $W > 3.1$ GeV (comparing with $b = 9.279$, which would give the same contribution in $\sigma(|\cos\theta^*| < 0.8)$ as the $\sin^{-4}\theta^*$ term does) although it becomes nearly constant and then systematically negative above the charmonium region. The change in the b parameter, which approaches a constant value near zero, occurs at a W value close to that observed in the charged pion case.

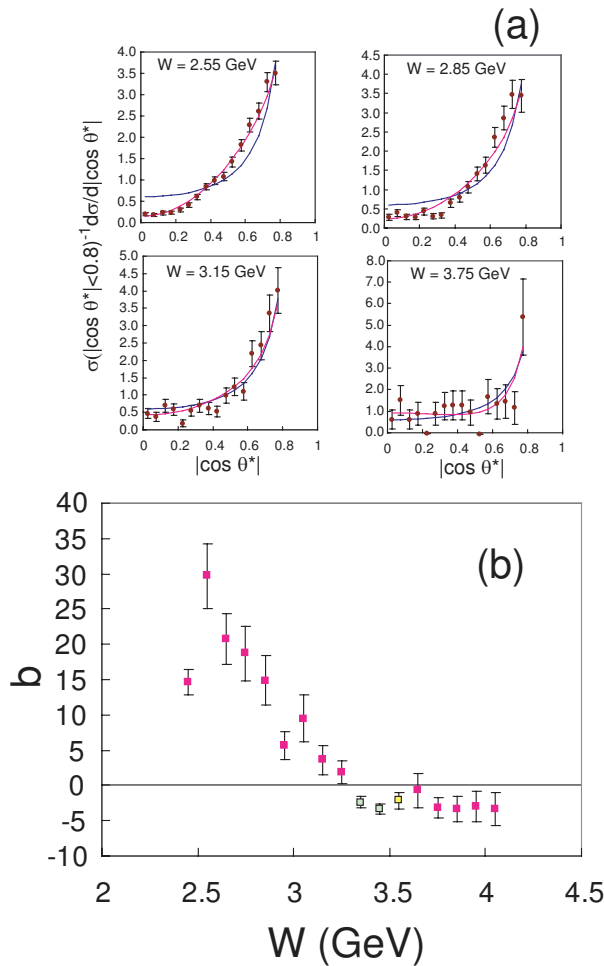


FIG. 6: (a) The fits of the angular dependence of the normalized DCS (see text) at four selected W points. For the blue curves the coefficient b (see the fit formula in the text) is fixed to 0. The magenta curves show the fits with b floating. (b) The energy dependence of the parameter b giving the best fits. Here, the charmonium contributions are not subtracted, and the data in the χ_{c0} and χ_{c2} charmonium regions are plotted with different colors.

B. Yields of χ_{cJ} charmonia

The structures seen in the yield distribution for $3.3 \text{ GeV} < W < 3.6 \text{ GeV}$ (Fig. 7) are from charmonium production, $\gamma\gamma \rightarrow \chi_{c0}$, $\chi_{c2} \rightarrow \pi^0\pi^0$. Similar production of the two charmonium states is observed in the $\pi^+\pi^-$, K^+K^- and $K_S^0K_S^0$ final states [2, 3].

We fit the distribution to contributions of χ_{c0} , χ_{c2} and a smooth continuum component, using the following function:

$$Y(W) = |\sqrt{\alpha k} W^{-\beta} + e^{i\phi} \sqrt{N_{\chi_{c0}}} \text{BW}_{\chi_{c0}}(W)|^2 + N_{\chi_{c2}} |\text{BW}_{\chi_{c2}}(W)|^2 + \alpha(1-k)W^{-\beta}, \quad (8)$$

in the W region between 2.8 and 4.0 GeV, where $\text{BW}_{\chi_{cJ}}(W)$ is a Breit-Wigner function for the charmonium amplitude, which is proportional to $\sim 1/(W^2 - M_{\chi_{cJ}}^2 - iM_{\chi_{cJ}}\Gamma_{\chi_{cJ}})$ and is normalized as $\int |\text{BW}_{\chi_{cJ}}(W)|^2 dW = 1$. The masses and widths, M and Γ , of the charmonium states are fixed to the PDG world averages [15]. The component $\alpha W^{-\beta}$ corresponds to

TABLE IV: Results of the fits (see text) to obtain the charmonium contributions with and without interference effects. Errors are statistical only. Logarithmic likelihood ($\ln \mathcal{L}$) values are only meaningful when comparing two or more fits.

Interference	$N_{\chi_{c0}}$	k	ϕ	$N_{\chi_{c2}}$	$-2 \ln \mathcal{L}/ndf$
Without	100 ± 16	—	—	13^{+11}_{-10}	52.4/56
With	103^{+60}_{-42}	$0.82^{+0.18}_{-0.48}$	$(1.1 \pm 0.3)\pi$	34 ± 13	44.2/54

the contribution from the continuum component, with a fraction k that interferes with the χ_{c0} amplitude with a relative phase angle, ϕ . It is impossible to determine the interference parameters for the χ_{c2} , because of its much smaller intrinsic width compared to the measurement resolution. We fit the χ_{c2} yield ($N_{\chi_{c2}}$) with a formula where no interference term is included, and later we estimate the maximum effects from the interference term when deriving the two-photon decay width of χ_{c2} . We use data only in the range $|\cos \theta^*| < 0.4$ where the charmonium contribution is dominant. We take into account the smearing effect due to a finite mass resolution in the fit, using the same function as used for the unfolding.

A binned maximum likelihood method is applied. We examined two cases with and without the interference. Reasonably good fits are obtained for both cases. The fit results are summarized in Table IV. In the table, \mathcal{L} is the likelihood value and ndf is the number of degrees of freedom. The normalization $N_{\chi_{c0}}$ in Eq.(8) is proportional to the square of the resonance amplitude. The yields from the fits are translated into products of the two-photon decay width and the branching fraction, $\Gamma_{\gamma\gamma}(\chi_{cJ})\mathcal{B}(\chi_{cJ} \rightarrow \pi^0\pi^0)$, which are listed in Table V. The systematic errors are taken from the changes in the best fits in the central values of yields when the absolute energy scale is varied by ± 10 MeV for the W measurement and the invariant-mass resolution is varied by $\pm 10\%$ for the corresponding Gaussian widths. The changes of the goodness of fit ($-2 \ln \mathcal{L}$) for these variations are found to be small, less than 1.7.

The χ_{c0} is observed with a statistical significance of 7.6σ (7.3σ) when we take (do not take) interference into account. The statistical significance for the χ_{c2} is 2.6σ when we take interference of the χ_{c0} into account, but it is only 1.3σ when we do not take into account interference. This is because interference makes the line shape of χ_{c0} highly asymmetric with a short tail and destructive interference on the high-energy side. The red and blue curves in Fig. 7 show the fits for the two cases of with and without χ_{c0} interference.

The results for $\Gamma_{\gamma\gamma}\mathcal{B}(\chi_{cJ})$ in the $\pi^0\pi^0$ final state are compared with previous measurements of $\Gamma_{\gamma\gamma}\mathcal{B}(\chi_{cJ})$ in the $\pi^+\pi^-$ decay mode, $15.1 \pm 2.1 \pm 2.3$ eV and $0.76 \pm 0.14 \pm 0.11$ eV for χ_{c0} and χ_{c2} , respectively [2], (or even $K\bar{K}$, referring to SU(3) symmetry [2, 3]) decay mode. Although the effects of interference were neglected in the $\pi^+\pi^-$ measurements, the results are consistent with the ratio expected from isospin invariance, $\mathcal{B}(\chi_{cJ} \rightarrow \pi^0\pi^0)/\mathcal{B}(\chi_{cJ} \rightarrow \pi^+\pi^-) = 1 : 2$.

TABLE V: Products of the two-photon decay width and the branching fraction for the two charmonia. Here, $\Gamma_{\gamma\gamma}\mathcal{B}(\chi_{cJ})$ means $\Gamma_{\gamma\gamma}(\chi_{cJ})\mathcal{B}(\chi_{cJ} \rightarrow \pi^0\pi^0)$. The first, second and third errors (if exists) are statistical, systematic and from the maximal uncertainties of the relative phase in χ_{c2} production.

Interference	$\Gamma_{\gamma\gamma}\mathcal{B}(\chi_{c0})$ (eV)	$\Gamma_{\gamma\gamma}\mathcal{B}(\chi_{c2})$ (eV)
Without	$9.7 \pm 1.5 \pm 1.0$	$0.18^{+0.15}_{-0.14} \pm 0.03$
With	$9.9^{+5.8}_{-4.0} \pm 1.0$	$0.48 \pm 0.18 \pm 0.05 \pm 0.14$

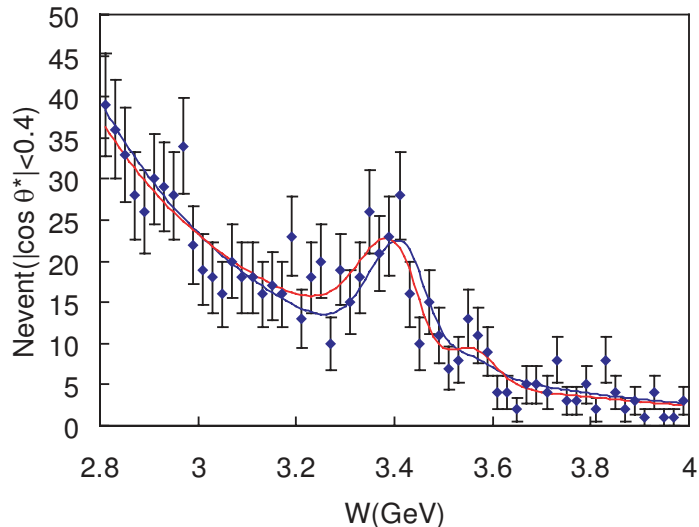


FIG. 7: The W distribution of the candidate events with $|\cos\theta^*| < 0.4$ near the charmonium region. The red and blue curves show the fits described in the text with and without interference with the χ_{c0} .

C. Subtraction of the charmonium contributions

We subtract the charmonium contributions from nearby bins of the charmonium (χ_{cJ}) region, 3.2 – 3.6 GeV, in order to obtain a pure DCS from the continuum component. We use the fit result with interference obtained in the previous subsection.

The estimated charmonium yield that includes the contribution from the interference term is converted to a DCS contribution in each angular bin of $|\cos\theta^*| < 0.8$ by assuming a flat distribution for the χ_{c0} component and a $\sim \sin^4\theta^*$ distribution for the χ_{c2} component [3]. This assumption is only a model. In reality, we do not know how the angular distribution of the interference term behaves; the charmonium amplitudes can interfere with the continuum components with different J 's of unknown sizes.

For the $W = 3.25$ GeV bin, the fit result indicates that there is a non-negligible effect from χ_{c0} when we assume interference, and thus we make a correction for charmonium subtraction. The contribution of the charmonium components in the original DCS is 18% at $|\cos\theta^*| < 0.6$. For $W = 3.3 - 3.6$ GeV, we apply subtraction for the angular bins

$0.4 < |\cos\theta^*| < 0.8$ after extrapolating the charmonium yield determined in the range $|\cos\theta^*| < 0.4$.

The DCS thus obtained for the continuum is integrated over the range $|\cos\theta^*| < 0.6$. We convert $\sigma(0.4 < |\cos\theta^*| < 0.8)$ to $\sigma(|\cos\theta^*| < 0.4)$ for $W = 3.3 - 3.6$ GeV, by assuming that the angular dependence of the DCS has a $\sim \sin^{-4}\theta^*$ dependence. The results are plotted in Fig. 8.

D. W dependence and cross-section ratio

We fit the DCS integrated over angle, $\sigma(|\cos\theta^*| < 0.6)$, to a power law in the c.m. energy, W^{-n} , for the energy region $3.1 \text{ GeV} < W < 4.1 \text{ GeV}$, in which the angular dependence of the DCS does not show any large changes. In the fit, we do not use the data in the charmonium region ($W = 3.3 - 3.6$ GeV), where we cannot determine the cross section of the continuum component in a model-independent manner.

The obtained result is $n = 6.9 \pm 0.6 \pm 0.7$. The systematic error is dominated by the uncertainty of the charmonium contribution in $3.1 \text{ GeV} < W < 3.3 \text{ GeV}$. This value is compatible with the results for the $\pi^+\pi^-$ and K^+K^- processes [2], but significantly different from the case of $K_S^0K_S^0$ [3].

The fit for $3.1 \text{ GeV} < W < 4.1 \text{ GeV}$ is shown in Fig. 8(a). We also show the ratio of $\pi^0\pi^0$ to $\pi^+\pi^-$ cross sections in Fig. 8(b). The two processes have a similar W^{-n} dependence for $3.1 \text{ GeV} < W < 4.1 \text{ GeV}$, while their ratio is almost constant in this energy region. The average of the ratio in this energy region is $\langle \text{Ratio} \rangle = 0.32 \pm 0.03 \pm 0.05$, where the data in the 3.3 - 3.6 GeV region is not used when calculating this average. This ratio is significantly larger than the prediction of the leading order QCD calculations [8, 9] and is slightly smaller than the value of 0.5, which appears in Ref. [10] based on isospin invariance.

VI. SUMMARY AND CONCLUSION

We have measured the process $\gamma\gamma \rightarrow \pi^0\pi^0$ based on data from e^+e^- collisions corresponding to an integrated luminosity of 223 fb^{-1} with the Belle detector at the KEKB accelerator. We derive results for the differential cross sections in the center-of-mass energy and polar angle ranges, $0.6 \text{ GeV} < W < 4.1 \text{ GeV}$ and $|\cos\theta^*| < 0.8$.

A simple model is employed to obtain some information on resonances up to $2.2 \text{ GeV}/c^2$. Differential cross sections are fitted in the energy region, $1.4 \text{ GeV} < W < 2.2 \text{ GeV}$, with a model where partial waves consist of resonances and smooth backgrounds. The G wave is seen to be important for $W > 1.8 \text{ GeV}$, where the G_2 wave appears to dominate over the G_0 wave [6]. Thus the $f_4(2050)$ is included in the G_2 wave while G_0 is set to zero. Parameters of the $f_2(1270)$ and other resonances are fixed at PDG [15] values and those determined in the previous analysis [1, 6]. Two solutions with reasonably good fit quality are obtained when an additional spin-2 resonance is introduced with a mass near $1.5 \text{ GeV}/c^2$ (denoted as $f_2(Z)$) in addition to the $f_2'(1525)$, $f_2(1950)$ and $f_4(2050)$. Without the $f_4(2050)$, the fit quality is unacceptable.

We observe production of the charmonium χ_{c0} state and obtain the product of its two-photon decay width and the branching fraction to $\pi^0\pi^0$. The energy and angular dependences above 3.1 GeV are compatible with those measured in the $\pi^+\pi^-$ channel, and we obtain the cross section ratio, $\sigma(\pi^0\pi^0)/\sigma(\pi^+\pi^-)$, to be $0.32 \pm 0.03 \pm 0.05$ on average in the 3.1-4.1 GeV

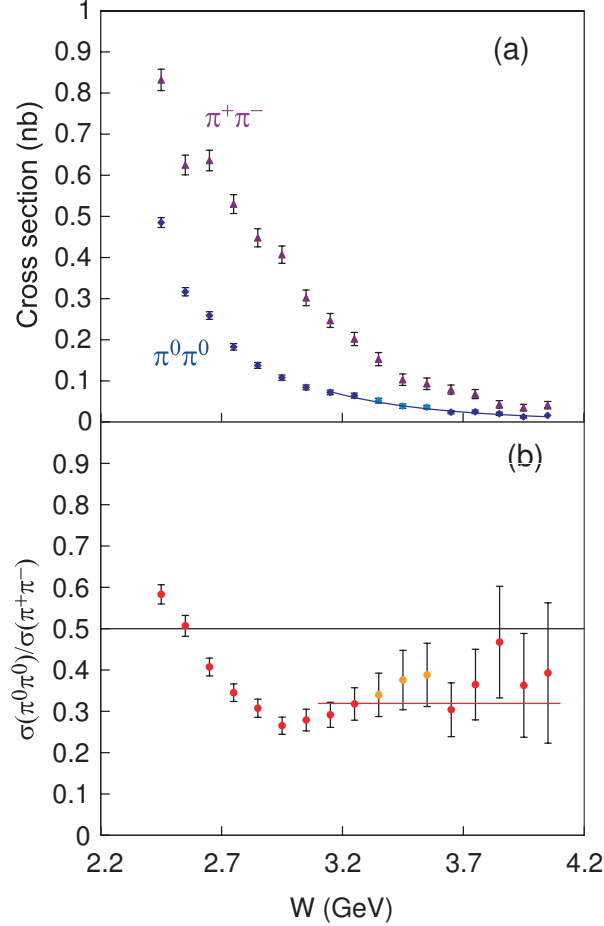


FIG. 8: (a) The cross sections for the $\gamma\gamma \rightarrow \pi^0\pi^0$ (blue diamonds) and $\gamma\gamma \rightarrow \pi^+\pi^-$ (violet triangles, [2]) for $|\cos\theta^*| < 0.6$. The curve is the fit to the cross section for $\gamma\gamma \rightarrow \pi^0\pi^0$ with a $\sim W^{-n}$ functional shape. (b) Ratio of the cross section of the $\pi^0\pi^0$ process to the $\pi^+\pi^-$ process. The error bars are statistical only. The red line is the average for $3.1 \text{ GeV} < W < 4.1 \text{ GeV}$. The horizontal line (0.5) is an expectation from isospin invariance for a pure $I = 0$ component. In (a) and (b), the estimated charmonium contributions are subtracted in both $\pi^+\pi^-$ and $\pi^0\pi^0$ measurements. The results in the W region 3.3 GeV - 3.6 GeV (plotted with lighter colors) are not used for the fits.

region. This ratio is significantly larger than the prediction of the leading order QCD calculation.

Acknowledgment

We thank the KEKB group for the excellent operation of the accelerator, the KEK cryogenics group for the efficient operation of the solenoid, and the KEK computer group and the National Institute of Informatics for valuable computing and SINET3 network support. We acknowledge support from the Ministry of Education, Culture, Sports, Science, and Technology of Japan and the Japan Society for the Promotion of Science; the Australian Research Council and the Australian Department of Education, Science and Training; the

National Natural Science Foundation of China under contract No. 10575109 and 10775142; the Department of Science and Technology of India; the BK21 program of the Ministry of Education of Korea, the CHEP src program and Basic Research program (grant No. R01-2005-000-10089-0, R01-2008-000-10477-0) of the Korea Science and Engineering Foundation; the Polish State Committee for Scientific Research; the Ministry of Education and Science of the Russian Federation and the Russian Federal Agency for Atomic Energy; the Slovenian Research Agency; the Swiss National Science Foundation; the National Science Council and the Ministry of Education of Taiwan; and the U.S. Department of Energy.

REFERENCES

- [1] Belle Collaboration, T. Mori *et al.*, Jour. Phys. Soc. Jpn. **76**, 074102 (2007); Belle Collaboration, T. Mori *et al.*, Phys. Rev. D **75**, 051101(R) (2007).
- [2] Belle Collaboration, H. Nakazawa *et al.*, Phys. Lett. B **615**, 39 (2005).
- [3] Belle Collaboration, W.T. Chen *et al.*, Phys. Lett. B **651**, 15 (2007).
- [4] Belle Collaboration, C.C. Kuo *et al.*, Phys. Lett. B **621**, 41 (2005).
- [5] Belle Collaboration, S. Uehara *et al.*, Phys. Rev. Lett. **96**, 082003 (2006).
- [6] Belle Collaboration, S. Uehara and Y. Watanabe *et al.*, Phys. Rev. D **78**, 052004 (2008).
- [7] Belle Collaboration, K. Abe *et al.*, BELLE-CONF-0768, arXiv.0711.1926 (2007).
- [8] S.J. Brodsky and G.P. Lepage, Phys. Rev. D **24**, 1808 (1981).
- [9] M. Benayoun and V.L. Chernyak, Nucl. Phys. B **329**, 209 (1990); V.L. Chernyak, Phys. Lett. B **640**, 246 (2006).
- [10] M. Diehl, P. Kroll and C. Vogt, Phys. Lett. B **532**, 99 (2002).
- [11] Belle Collaboration, A. Abashian *et al.*, Nucl. Instr. and Meth. A **479**, 117 (2002).
- [12] S. Kurokawa and E. Kikutani, Nucl. Instr. and Meth. A **499**, 1 (2003), and other papers included in this volume.
- [13] A. Höcker and V. Kartvelishvili, Nucl. Instr. Meth. A **372**, 469 (1996).
- [14] S. Uehara, KEK Report 96-11 (1996).
- [15] Particle Data Group, C. Amsler *et al.*, Phys. Lett. B **667**, 1 (2008), and the web update (2008).